Inorganic Chemistry

pubs.acs.org/IC
Article

Synthesis and Characterization of Cerium-Oxo Clusters Capped by Acetylacetonate

Anamar Blanes-Díaz, Mohammad Shohel, Natalie T. Rice, Ida Piedmonte, Morgan A. McDonald, Kaveh Jorabchi, Stosh A. Kozimor, Jeffery A. Bertke, May Nyman, and Karah E. Knope*

Cite This: https://doi.org/10.1021/acs.inorgchem.3c02141

ABSTRACT: Cerium-oxo clusters have applications in fields ranging from catalysis to electronics and also hold the potential to inform on aspects of actinide chemistry. Toward this end, a cerium-acetylacetonate ($acac^{1-}$) monomeric molecule, $Ce(acac)_4$ (**Ce-1**), and two $acac^{1-}$-decorated cerium-oxo clusters, $[Ce_{10}O_8(acac)_{14}(CH_3O)_6(CH_3OH)_2]\cdot 10.5MeOH$ (**Ce-10**) and $[Ce_{12}O_{12}(OH)_4(acac)_{16}(CH_3COO)_2]\cdot 6(CH_3CN)$ (**Ce-12**), were prepared and structurally characterized. The $Ce(acac)_4$ monomer contains Ce^{IV}. Crystallographic data and bond valence summation values for the **Ce-10** and **Ce-12** clusters are consistent with both clusters having a mixture of Ce^{III} and Ce^{IV} cations. Ce L_3-edge X-ray absorption spectroscopy, performed on **Ce-10**, showed contributions from both Ce^{III} and Ce^{IV}. The **Ce-10** cluster is built from a hexameric cluster, with six Ce^{IV} sites, that is capped by two dimeric Ce^{III} units. By comparison, **Ce-12**, which formed upon dissolution of **Ce-10** in acetonitrile, consists of a central decamer built from edge sharing Ce^{IV} hexameric units, and two monomeric Ce^{III} sites that are bound on the outer corners of the inner Ce_{10} core. Electrospray ionization mass spectrometry data for solutions prepared by dissolving **Ce-10** in acetonitrile showed that the major ions could be attributed to Ce_{10} clusters that differed primarily in the number of $acac^{1-}$, OH^{1-}, MeO^{1-}, and O^{2-} ligands. Small angle X-ray scattering measurements for **Ce-10** dissolved in acetonitrile showed structural units slightly larger than either Ce_{10} or Ce_{12} in solution, likely due to aggregation. Taken together, these results suggest that the acetylacetonate supported clusters can support diverse solution-phase speciation in organic solutions that could lead to stabilization of higher order cerium containing clusters, such as cluster sizes that are greater than the Ce_{10} and Ce_{12} reported herein.

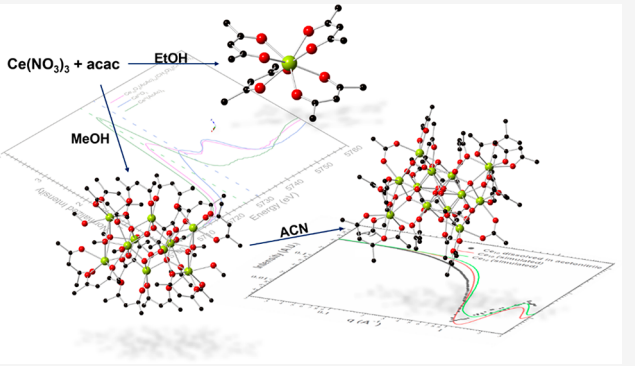

INTRODUCTION

Cerium-based materials have found application in areas ranging from catalysis to downconverters in light emitting diodes.[1−7] These applications, together with the relative abundance and low cost of cerium, have motivated efforts focused on structure−property relationships and hence materials development. Among cerium compounds, CeO_2 (ceria) stands out as having uniquely diverse properties. One of the most notable industrial applications of ceria is its use in three-way catalysts (TWCs); ceria can serve several purposes for TWCs, including acting as an oxygen storage component due to its reduction potential.[8,9] In fact, the accessibility of the +3 and +4 oxidation states prompts many efforts that seek to harness the redox chemistry of cerium toward uses in optics, solid-oxide fuels, and oxygen storage.[10−12] Largely motivated to (1) better understand the catalytic behavior of CeO_2 and (2) develop novel Ce-based catalysts that can be fine-tuned for specific applications, the chemistry community has become interested in cerium-oxo clusters. These species can be regarded as molecular scale nanoparticles of CeO_2, and their properties seem to depend on the nuclearity and composition of the Ce cluster.[13] As a testament, Christou et al. recently demonstrated the ability of Ce-oxo clusters to scavenge reactive oxygen species, and the activity of these clusters was dependent on the number of Ce^{III} atoms present in the cluster.[14] It seems likely that the catalysis applications space for Ce-oxo clusters is wide and diverse because there are a large number of Ce-oxo clusters that can be prepared. For example, synthetic chemists have discovered reproducible synthetic methods for molecules that have between two cerium atoms (homometallic dimers; Ce_2) and clusters with up to one hundred cerium atoms (Ce_{100}). In an attempt to further diversify the landscape of Ce-oxo cluster chemistry, new

Special Issue: Ligand-Metal Complementarity in Rare Earth and Actinide Chemistry

Received: June 27, 2023

avenues in Ce-oxo cluster synthesis are currently being explored by many research teams.[6,14−25]

In addition to serving as a platform for realizing novel materials properties, Ce-oxo clusters may also provide important insight into the chemical behavior of the lower valent actinides.[26,27] Cerium has historically served as a surrogate for plutonium, owing to similarities in ionic radii and accessible +3 and +4 oxidation states.[28−32] Specifically regarding cluster chemistry, there are several phases, including the M_6-, M_{22}-, and M_{38}-oxo clusters, that have been isolated for both Ce and Pu ions.[20,24,25,33−35] Similarities between Ce and Pu suggest that Ce may serve as a potential guide for expanding Pu cluster chemistry. The latter is significant because nanosized Pu-oxo cluster chemistry is of potential relevancy for plutonium processing chemistry and fate and transport in the environment.[36−39] In this regard, defining Ce-oxo cluster chemistry will advance our overall understanding of lanthanide vs actinide cluster chemistry, thereby improving our ability to control the chemistry of f-element oxo-clusters and advance our predictive capabilities in this area. Indeed, the potential translatability of Ce to actinide cluster chemistry motivates our current efforts.

Previously, our group reported the synthesis and characterization of a Ce_{38}-oxo cluster that was isolated from halide media using K^{1+} counterions.[24] The compound was prepared through evaporation and exhibited a solid-state phase transformation that underscored the surface lability and reactivity of chloride ligated Ce-oxo clusters. Herein, we sought to limit synthetic challenges by controlling the surface lability and Ce redox chemistry. We achieved this control by leveraging nonaqueous alcoholic solutions and through the use of acetylacetonate ($acac^{1-}$) as a bidentate cluster capping agent. Note, $acac^{1-}$ has been used previously in lanthanide cluster chemistry.[40,41] Toward this end, we examined reactions between cerium and $acac^{1-}$ in alcoholic solvents: methanol and ethanol. We then developed synthetic methodology for monomeric $Ce(acac)_4$ as well as for two novel $acac^{1-}$ capped clusters: $[Ce_{10}O_8(acac)_{14}(CH_3O)_6(CH_3OH)_2]\cdot 10.5MeOH$ (**Ce-10**) and $[Ce_{12}O_{12}(OH)_4(acac)_{16}(CH_3COO)_2]\cdot 6(CH_3CN)$ (**Ce-12**). The structures were characterized by single-crystal X-ray diffraction. Bond valence summation values for the Ce sites[42,43] suggested that $Ce(acac)_4$ contained Ce^{IV}, **Ce-10** contained both Ce^{III} and Ce^{IV}, and **Ce-12** also contained Ce^{III} and Ce^{IV}. Examination of **Ce-10** using X-ray absorption spectroscopy (XAS) was consistent with the mixed oxidation state Ce^{III}/Ce^{IV} formulation. The vibrational properties of the compounds are also described. The stability of the **Ce-10** cluster in solution was examined via ^1H NMR spectroscopy, small-angle X-ray scattering (SAXS), and electrospray ionization mass spectrometry; these data suggest that upon dissolution in acetonitrile, **Ce-10** aggregates into particles with a larger average size than the **Ce-10** and **Ce-12** clusters. Overall, this work points to the utility of β-diketonate ligands in the isolation of Ce-oxo clusters and the importance of solvent on cluster topology. The latter is evidenced by the precipitation of monomers from ethanol, decamers from methanol, and dodecamers from acetonitrile. This observation highlights the unique solvent role in Ce-oxo formation, and we are excited at the prospect of better defining solvent effects in the following studies. Moreover, given the simplicity and facile reproducibility of the synthesis, this organic system may be an entry to differentiating cluster chemistry for plutonium and, potentially, other actinide elements.

EXPERIMENTAL SECTION

Materials. The following chemicals were purchased from commercial suppliers and used as received: $Ce(NO_3)_3\cdot 6H_2O$ (ACROS Organics), acetylacetone (Hacac; TCI America), methanol (Fisher Chemical), 200 proof ethanol (The Warner-Graham Company), triethylamine (Sigma-Aldrich), acetonitrile (MeCN; Fisher Chemical), and hexanes (Fisher Chemical). All of the following reactions were performed under ambient conditions.

Synthetic Details. Compound **Ce-1**, $Ce(acac)_4$, was obtained by dissolving $Ce(NO_3)_3\cdot 6H_2O$ (0.3262 g, 1 mmol) and Hacac (204 μL, 2 mmol) in EtOH (3 mL) in a glass vial (7 mL). The solution was sonicated for five min, and then triethylamine (557 μL, 4 mmol) was added dropwise to the solution. The solution was then cooled to 15 °C. After 1 week, orange, rod-like crystals of **Ce-1** and an unidentified yellow−orange powder had precipitated. The mother liquor was removed from the vial, and the reaction product was washed (3 × 3 mL) with a one-to-one mixture of EtOH-to-hexanes. The crystals were left to dry under ambient conditions (1 h). Note that based on visual inspection and PXRD (Figure S13), **Ce-1** was a minor phase in the reaction product.

Compound **Ce-10**, $[Ce_{10}O_8(acac)_{14}(CH_3O)_6(CH_3OH)_2]\cdot 10.5MeOH$, was prepared using various synthetic conditions, as detailed in the Supporting Information. The synthesis described here is readily reproducible and yields a pure phase. $Ce(NO_3)_3\cdot 6H_2O$ (0.3262 g, 1 mmol) and Hacac (204 μL, 2 mmol) were added to a glass vial (7 mL) that contained MeOH (3 mL). The solution was sonicated (5 min) until the $Ce(NO_3)_3\cdot 6H_2O$ dissolved. Once dissolved, triethylamine (557 μL, 4 mmol) was added dropwise to yield a dark-orange solution. The solution was then capped and cooled to 15 °C. After 24 h, orange crystals formed, and the mother liquor was removed. The crystals were washed (3 × 3 mL) with a one-to-one mixture of MeOH-to-hexanes. Then the crystals were left to dry under ambient conditions (1 h). Yield based on Ce: 20%. Elemental analysis calc (obs) C: 29.60 (29.81), H: 3.89 (3.88).

Compound **Ce-12**, $[Ce_{12}O_{12}(OH)_4(acac)_{16}(CH_3COO)_2]\cdot 6(MeCN)$, was obtained by combining $[Ce_{10}O_8(acac)_{14}(CH_3O)_4(CH_3OH)_4]\cdot 10.5MeOH$ (**Ce-10**, 10 mg, 0.003 mmol) and acetonitrile (0.5 mL) in a glass vial (7 mL). A yellowish−brown suspension formed after the mixture was sonicated (10 min). The vial was capped, and after 1 week, yellow single crystals (rod shaped) of **Ce-12** formed alongside an unidentified light brown powder. Note that the compound is formulated with two acetate ligands that are presumed to form *in situ*, vide infra.

Structure Determination by Single Crystal X-ray Diffraction. Crystals of **Ce-1**, **Ce-10**, and **Ce-12** were isolated from the bulk reaction products and mounted on MiTeGen loops in Paratone oil. Single crystal X-ray diffraction data were collected at 100 K on a Bruker D8 Quest diffractometer equipped with a Mo Kα microfocus source (λ = 0.71073 Å), an Oxford 700 Cryostream, and a Photon100 detector. The data were integrated using the SAINT software package included in APEX3, and absorption corrections were applied using a multiscan technique in SADABS. The structures were solved using SHELXT and refined by full matrix least-squares on F2 using SHELXL software on shelXle64.[44−48] Crystal data and structure refinement details are provided in Table 1; further details of the structure refinements are provided in the Supporting Information.

Bulk Solid-State Characterization Methods. Powder X-ray diffraction data for the bulk samples from which crystals of **Ce-1**, **Ce-10**, and **Ce-12** were isolated were obtained using Cu−Kα radiation (λ = 1.542 Å) on a Rigaku Ultima IV X-ray diffractometer from 3 to 40° in 2θ with a step speed of 1 degree/min (Figures S13−S15). IR spectra for **Ce-10** and **Ce-12** were collected on single crystals using a Nicolet iN10 Infrared Microscope FTIR-ATR with a Ge ATR tip over $\Delta\nu$ 675−4000 cm^{-1} (Figures S17−S18). For **Ce-10**, combustion elemental analysis was performed on the bulk sample by using a PerkinElmer model 2400 elemental analyzer.

X-ray Absorption Spectroscopy (XAS). A sample of **Ce-10**, and oxidation state standards, CeO_2 and $Ce(acac)_3\cdot(H_2O)_x$, were prepared as detailed in the Supporting Information. Ce L_3-edge

https://doi.org/10.1021/acs.inorgchem.3c02141
Inorg. Chem. XXXX, XXX, XXX−XXX

Table 1. Crystallographic Structure Refinement Details for Ce-1, Ce-10, and Ce-12

	Ce-1	Ce-10	Ce-12
Formula	$C_{30}H_{28}CeO_8$	$C_{78}H_{122}Ce_{10}O_{44}$	$[C_{84}H_{118}Ce_{12}O_{52}](C_2H_3N)_6$
MW (g mol^{-1})	536.54	3164.95	3887.54
T (K)	100	100	100
crystal color/ habit	orange rod	orange block	yellow block
crystal system	monoclinic	monoclinic	triclinic
λ (Å)	0.71073	0.71073	0.71073
Space group	$C2/c$	$P2_1/n$	P-1
a (Å)	21.5200(13)	14.7545(8)	14.173(5)
b (Å)	8.3715(5)	20.6763(11)	16.254(6)
c (Å)	13.9042(9)	20.1617(11)	16.770(9)
α (deg)	90	90	112.390(14)
β (deg)	114.353(2)	108.647(2)	108.333(18)
γ (deg)	90	90	98.191(13)
V (Å^3)	2282.0(2)	5827.8(5)	3236(3)
Z	2	2	2
ρ (mg m^{-3})	1.562	1.804	1.995
μ (mm^{-1})	2.035	3.892	4.209
R_1	0.0184	0.0484	0.0448
wR_2	0.095	0.1017	0.1477
GOF	1.414	1.028	1.035
CCDC	2257004	2257005	2257002

XAS data were collected in transmission mode using an in-house XAS spectrometer at Los Alamos National Laboratory.[49] Fifty scans were obtained and averaged per cerium sample, and four scans were obtained and averaged for the Cr foil (used for energy calibration). Data manipulation and analysis were conducted as previously described by Solomon and co-workers.[50] Further details on the instrument configuration, data collection, and data analysis are available in the Supporting Information.

Solution State Characterization Methods. *Small Angle X-ray Scattering (SAXS).* X-ray scattering data were collected on an Anton Paar SAXS instrument using Cu−Kα radiation (1.54 Å) equipped with line collimation. A 2-D image plate was used for data collection in the q = 0.018−2.5 Å^{-1} range. The lower q resolution is limited by the beam attenuator. The solution obtained by dissolving **Ce-10** in acetonitrile was filtered with a 0.45 μm membrane filter and then filled in a 1.5 mm glass capillary (Hampton Research) for the SAXS measurement. Scattering data of neat solvent were also collected for background subtraction. Scattering was measured for 30 min for each experiment. SAXSQUANT software was used for data collection and post processing (normalization, primary beam removal, background subtraction, desmearing, and smoothing to remove extra noise created by the desmearing routine). Data were analyzed using IRENA macros with IgorPro 6.3 (Wavemetrics) software.[51] Simulated scattering patterns of the **Ce-10** and **Ce-12** clusters were generated using SolX utilizing structural files (.xyz) containing a selected portion of the structure that did not include solvent or coordinated ligands.[52]

^{1}H Nuclear Magnetic Resonance Spectroscopy. Crystals of **Ce-10** were dissolved in deuterated acetonitrile (CD_3CN) and filtered through Celite. A ^{1}H NMR spectrum was then collected using a Varian 400-MR NMR. The spectrum (Figure S22) and peak assignments (Table S6) are provided as Supporting Information.

Electrospray Ionization Mass Spectrometry. Mass spectra were collected by using nanospray ionization and a quadrupole time-of-flight instrument (QStar XL, Sciex, Ontario, Canada). Crystals of **Ce-10** (4.5 mg) were dissolved in acetonitrile, and the solution was diluted to approximately 50 μM. The sample solution was then loaded into a pulled borosilicate capillary (1 mm o.d. 0.75 mm i.d. pulled to 5 μm tip size) with its tip placed ∼1 cm from the curtain plate inlet of the mass spectrometer. A platinum electrode was inserted into the back of the capillary to make electrical contact with the solution for nanospray generation. Voltages of 2200−2400 V were applied to the solution while the spectrometer plate was held at 1100 V. The instrument was operated in TOF mode without any collision-induced dissociation gas in Q2 using DP1 = 50 V and DP2 = 10 V. These conditions produced a gentle ion sampling while helping desolvate the noncovalently bound solvent molecules.

RESULTS AND DISCUSSION

Structure Descriptions. Compound **Ce-1**, $Ce(acac)_4$, crystallized in the monoclinic space group, $C2/c$. The structure consists of a Ce^{IV} monomeric unit, $Ce(acac)_4$, that is composed of an eight-coordinate cerium(IV) metal center bound to oxygen atoms from four $acac^{1-}$ ligands as shown in Figure 1. The $acac^{1-}$ ligands bind in a bidentate fashion, with

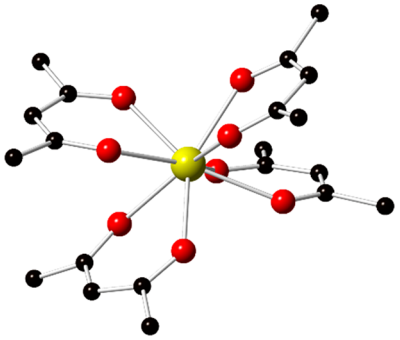

Figure 1. Ball and stick illustration of the $Ce(acac)_4$ monomer. Ce is shown in yellow, O in red, and C in black. Hydrogen atoms have been removed for clarity.

Ce−O bond distances ranging from 2.311(2)−2.348(2) Å. Note that **Ce-1** is isostructural with a $Ce(acac)_4$ monomer reported by Matkovic and Grdenic;[53] however, the compound crystallizes with a different unit cell.

Compound **Ce-10**, $[Ce_{10}O_8(acac)_{14}(CH_3O)_6(CH_3OH)_2]\cdot 10.5$ MeOH, crystallized in the $P2_1/n$ space group. Five crystallographically unique Ce sites constitute the structure of **Ce-10**. Further details on metal ion coordination numbers and Ce−O bond lengths are provided in the Supporting Information (Table S2). Overall, the structure is built from a decameric $[Ce_6^{IV}Ce_4^{III}O_8(OMe)_4]^{16+}$ cluster core (Figure 2), wherein ten Ce sites are bridged by eight μ_3/μ_4-oxo dianions and four μ_3-OMe^{1-} monoanions. Bond valence summation values, which are the sum of the individual valences for an atom that add up to the oxidation state,[54] calculated for the **Ce-10** cluster were consistent with six Ce^{IV} and four Ce^{III} sites (Table S7). The Ce^{IV} sites are located at the center of the Ce_{10} core and adopt an oxo-bridged hexanuclear moiety with six Ce^{IV} cations connected by eight oxo-ligands; related structural units have been reported for both trivalent (e.g., Bi and Ce) and tetravalent (e.g., Zr, Hf, Th, U, Np, Pu) metal ions.[35,55−70] By comparison, the Ce^{III} sites form methoxy-bridged dinuclear $[Ce_2(OMe)_2]$ species and two of these structural units "cap" the hexamer via bridging μ_4-oxo groups to generate the decameric cluster shown in Figure 2. Fourteen $acac^{1-}$ ligands, two OMe^{1-}, and two MeOH ligands bind the cluster core (Figure 2b).

Dissolution of **Ce-10** in acetonitrile reproducibly generated compound **Ce-12**, $[Ce_{12}O_{12}(OH)_4(acac)_{16}(CH_3COO)_2]\cdot 6(CH_3CN)$, which crystallized in the triclinic space group, *P-1*. Overall, the structure is composed of a Ce_{12}-oxo/hydroxo cluster, $[Ce^{IV}{}_{10}Ce^{III}{}_2O_{12}(OH)_4]^{18+}$, that is ligated by 16 $acac^{1-}$

https://doi.org/10.1021/acs.inorgchem.3c02141
Inorg. Chem. XXXX, XXX, XXX−XXX

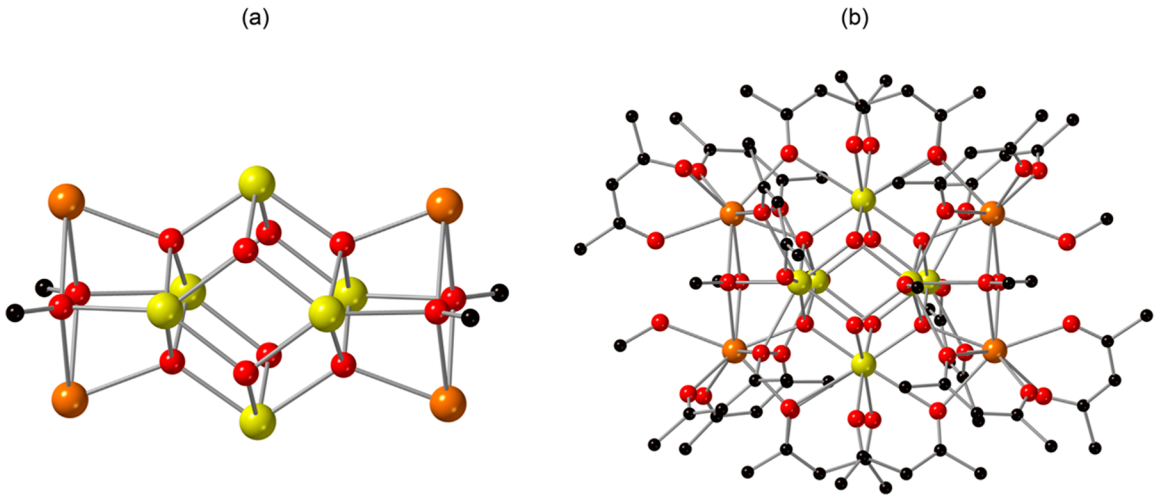

Figure 2. Illustration of the Ce_{10} cluster of **Ce-10** (a) highlighting the $[Ce_6^{IV}Ce_4^{III}O_8(Ome)_4]^{16+}$ core; Ce^{III} and Ce^{IV} sites are shown in orange and yellow, respectively, and (b) showing the $acac^{1-}$ decorated $[Ce_{10}O_8(acac)_{14}(CH_3O)_6(CH_3OH)_2]$ cluster. Ce is shown in yellow and orange, O in red, and C in black.

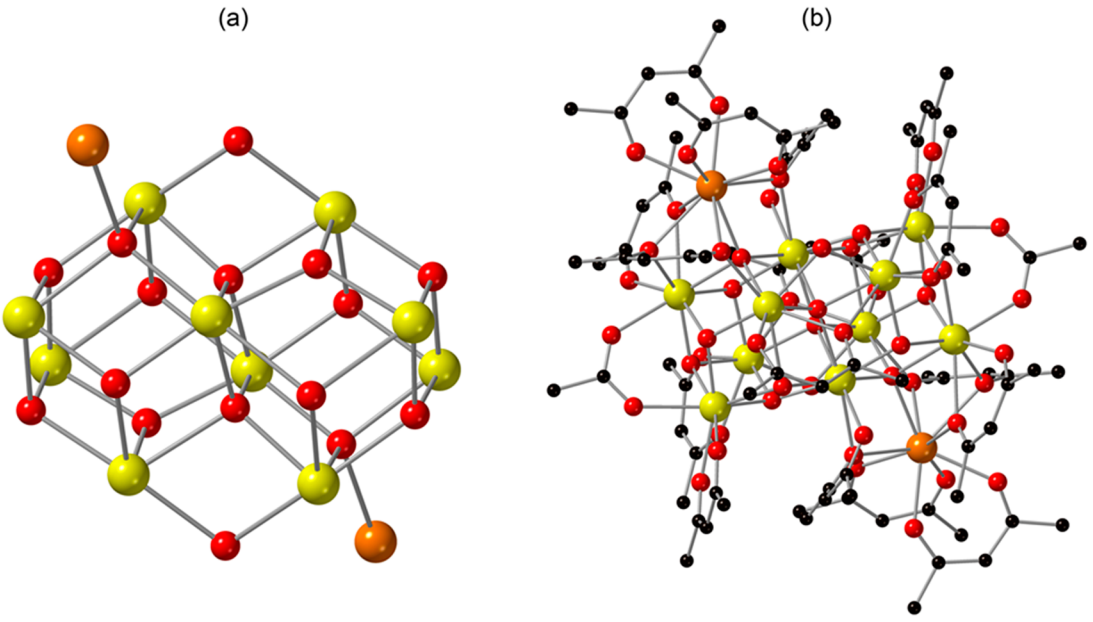

Figure 3. Illustration of **Ce-12** highlighting (a) the $[Ce^{IV}{}_{10}Ce^{III}{}_2O_{12}(OH)_4]^{18+}$ cluster core that consists of both Ce^{III} (orange) and the Ce^{IV} (yellow) sites and (b) the $acac^{1-}$ and acetate decorated $[Ce_{12}O_{12}(OH)_4(acac)_{16}(CH_3COO)_2]$ cluster. Ce is shown in yellow and orange, O in red, and C in black. Acetonitrile molecules that reside in the lattice have been omitted for clarity.

and two acetate groups to give a neutral cluster (Figure 3). Within the cluster, there are six crystallographically unique Ce sites, one of which (Ce1) is Ce^{III} and five of which (Ce2−Ce6) are Ce^{IV} based on BVS values (Table S10). As shown in Figure 3a, the five Ce^{IV} metal centers, together with their symmetry equivalent sites, are bridged through two μ_2-hydroxo, two μ_3-hydroxo, ten μ_3-oxo, and two μ_4-oxo groups to form a decameric unit that can be described as two edge-sharing Ce_6 octahedra. These octahedra are linked through two μ_4-oxo sites. The two Ce^{III} metal centers are located at opposite sides of the Ce_{10} core (related by an inversion center) to yield the Ce_{12} structural unit; the Ce^{III} cations bind through two μ_3-oxo ions (of the Ce_{10} unit), which become μ_4-oxo via coordination of the Ce^{III} sites. Location of the Ce^{III} metal centers at the periphery of the cluster is consistent with previous reports of Ce cluster chemistry,[24,71] as well as the structure of compound **Ce-10**. As shown in Figure 3b, the $[Ce^{IV}{}_{10}Ce^{III}{}_2O_{12}(OH)_4]^{18-}$ cluster is further coordinated to 16 $acac^{1-}$ and two acetate ligands, with the latter presumably forming *in situ* through oxidative cleavage of the $acac^{1-}$.[72] Additionally, six acetonitrile molecules are present in the lattice (Figure S11). Further details on metal ion coordination numbers, Ce−O bond distances, and Ce−OH bond lengths are provided in the Supporting Information (Table S3).

Relationship to Other Ce-Oxo Clusters. Cerium cluster chemistry has seen a significant expansion over the past two decades.[18,20,24,73−78] The **Ce-10** and **Ce-12** clusters exhibit unique arrangements of Ce metal centers that previously have not been reported. Nonetheless, some features of the clusters compare well with those of other known clusters. As summarized in the Supporting Information (Table S12), the most common core motif reported for Ce is the hexameric unit

https://doi.org/10.1021/acs.inorgchem.3c02141
Inorg. Chem. XXXX, XXX, XXX−XXX

of composition $[Ce_6O_4(OH)_4]^{12+}$.[14,18,24,77,79] This cluster has most frequently been isolated using carboxylate donors, and the Ce sites are usually tetravalent. Notably, the pervasiveness of the hexanuclear entity is similarly reflected in the cluster chemistry of other +3 and +4 metal ions including Bi^{III}, Zr^{IV}, Hf^{IV}, Th^{IV}, U^{IV}, Np^{IV}, and Pu^{IV}.[35,64,65,80]

The Ce_6 octahedral core manifests in both the **Ce-10** and **Ce-12** clusters reported herein. As noted above, the Ce_{10} assembly in **Ce-10** consists of a central Ce^{IV}_6 oxo bridged moiety that is effectively capped by two methoxy bridged Ce^{III} dimers to generate a decamer. By comparison, **Ce-12** is composed of edge-sharing Ce^{IV} octahedra; two Ce^{III} monomers are located at opposite ends of the core. The observation of the Ce_6 unit as a component of larger assemblies is similarly reflected in the literature. For example, Christou et al. recently reported $(pyH)_8[Ce_{10}O_4(OH)_4(O_3PPh)_{12}(NO_3)_{12}]$ that consisted of a face capped $[Ce_6O_4(OH)_4]^{12+}$ core.[77] Additionally, Loiseau et al. reported a Ce dodecamer, $[\{Ce_6(\mu_3\text{-}O)_4(\mu_3{-}OH)_3(\mu_4\text{-}O)_2\text{-}Ce_6(\mu_3\text{-}O)_4(\mu_3OH)_3\}(CH_3COO)_{13}(SiW_9O_{34})_2]^{11-}$, that is perhaps best described as two hexameric units bridged via oxo groups.[81]

In addition to previously reported homometallic Ce_{10} decamers,[77] which exhibit different arrangements of Ce atoms as compared to **Ce-10**, there are few heterometallic assemblies that consist of Ce_{10} assemblies together with other metal ions such as Mn and Na.[20,82−84] These Ce_{10} cluster cores vary in the arrangement of the Ce metal centers and range from edge-sharing Ce_6 octahedra to three Ce_3 units surrounding a central Ce site.[20,82−84] Interestingly, the homo- and heterometallic structures that consist of edge-sharing Ce_6 octahedra, such as $(pyH)_8[Ce_{10}O_4(OH)_4(O_3PPh)_{12}(NO_3)_{12}]$ and $[Ce_{10}Mn_{14}O_{24}(O_2CPh)_{32}]$, adopt the same decameric unit that is observed in **Ce-12**. Such units have likewise been observed for the actinides.[85,86] For example, $[U_{10}O_8(OH)_6(PhCO_2)_{14}I_4(H_2O)_2(MeCN)_2]$ consists of edge-sharing octahedra.[86] Dodecameric species have previously been reported for lanthanide ions including Pr, Nd, Gd, and Dy.[87−91] Yet there are only a handful of homo- and heterometallic Ce_{12} units reported.[5,81,87,88,92] Perhaps most notably, $Ce_{12}(C_2)_3I_{17}$ adopts a similar core to that observed in compound **Ce-12**.[87] However, although the cluster in **Ce-12** exists as an isolated structural unit, $Ce_{12}(C_2)_3I_{17}$ adopts extended chains with C_2 units in interstitial positions.

Finally, it is worth noting the location of the Ce^{III} and Ce^{IV} sites in the clusters. It is fairly well established in the cerium literature that for mixed oxidation state clusters, Ce^{III} and Ce^{IV} tend to locate to the cluster surface and core, respectively.[18] Indeed, the oxidation state assignments of the Ce sites in **Ce-10** and **Ce-12** based on bond valence summation values are consistent with literature precedence.[71] For **Ce-10**, the Ce^{IV} sites form a hexanuclear core that is capped by Ce^{III} dimers. Compound **Ce-12** has a similar arrangement of Ce^{III} and Ce^{IV} sites, with ten Ce^{IV} forming edge-sharing octahedra, and two Ce^{III} located at the periphery of the cluster. This tendency is also manifested in heterometallic clusters. For example, Gupta et al. characterized $[Ce_6Mn_{12}O_{17}(O_2CPh)_{26}]$, which consisted of four $\{Mn_3(\mu_3\text{-}O)_2\}$ surrounding a Ce^{IV}_6 core.[93] Likewise, Thuijs et al. reported $[Ce_3Mn_8O_8(O_2CPh)_{18}(HO_2CPh)_2]$ for which the central position in the cluster core was occupied by Ce^{IV} and the surface was composed of two Ce^{III} and eight Mn^{III} sites.[94] Nonetheless, it is important to note that this is not the only arrangement observed. For example, Kögerler et al. reported a Ce decamer that consisted of Ce^{IV} cations surrounding a central Ce^{III}.[20]

Synthetic Considerations. An interesting attribute associated with the formation of **Ce-10** was that its formation was dependent on the solvent identity and the cerium starting material used in the reaction. For example, monomeric $Ce(acac)_4$ was isolated from ethanolic solutions. Meanwhile, **Ce-10** that consists of methoxy bridged units was isolated from methanolic solutions. We rationalized these results based on the realization that methanol is more acidic than ethanol, which can explain why a methoxide is formed and the ethoxide equivalent does not form.[95] Interestingly, the **Ce-10** cluster was pervasive across a range of reaction conditions as detailed in the Supporting Information. The structural unit was found to precipitate irrespective of the Ce source. For example, Ce^{III}-chloride, nitrate, triflate, and sulfate salts as well as $Ce^{IV}(SO_4)_2$ all generated the **Ce-10** cluster. Thus, **Ce-10** formed irrespective of the Ce oxidation state in the starting materials, with oxidation of Ce^{III} possibly occurring by action of ambient O_2,[96] and reduction of Ce^{IV} plausibly occurring via oxidation of $acac^{1-}$, as reported previously.[97,98] In addition to **Ce-10**, two other structures built from **Ce-10** were isolated (see Supporting Information). These phases differ primarily in packing due to differences in solvent inclusion into the lattice. Finally, **Ce-12** was prepared through dissolution of **Ce-10** in MeCN, and efforts to synthesize the phase from cerium salts were unsuccessful. The ^{1}H NMR and SAXS data are consistent with rearrangement of the structural units in solution and ligand dissociation from the cluster. Peaks in the ^{1}H NMR spectrum (Figure S22; Table S6) are observed at approximately 3.6, 5.45, and 5.6 ppm and are attributed to free Hacac (3.6 and 5.6 ppm) and bound $acac^{1-}$ (5.45 ppm, 5.6 ppm).[99] The presence of acetate ligands in **Ce-12** may result from oxidative cleavage of $acac^{1-}$, *in situ*. Such oxidative cleavage has previously been reported in MeCN using mild catalysts such as quaternary ammonium iodide and H_2O_2.[72] The oxidative cleavage of $acac^{1-}$ to yield acetate in this work points to the reactivity of the Ce clusters.

Vibrational Spectroscopy. The infrared (IR) spectra for **Ce-10** (Figure S20) and **Ce-12** (Figure S21) are reported. The spectra are dominated by vibrations attributed to $acac^{1-}$. Assignments are provided in Tables S4 and S5.

^{1}H Nuclear Magnetic Resonance Spectroscopy. A ^{1}H NMR spectrum was collected for the solution obtained by adding **Ce-10** to deuterated acetonitrile (Figure S22), mimicking the procedure used to obtain **Ce-12**. The peak observed at approximately 3.6 ppm is consistent with the keto form of free Hacac, and the peak at 5.45 ppm is assigned to bound $acac^{1-}$. The peak at approximately 5.6 ppm may be attributed to the enol tautomer of Hacac or bound $acac^{1-}$. These assignments point toward evidence of ligand dissociation of **Ce-10** when dissolved in solution, and SAXS, discussed below, points to species larger than **Ce-10** or **Ce-12** in solution. Crytals of **Ce-12** precipitate from the solution, along with an amorphous material that is likely cerium oxyhydroxide.

Small Angle X-ray Scattering (SAXS). We conducted SAXS experiments to determine if any information could be gleaned about the stability of **Ce-10** in acetonitrile and/or the formation of **Ce-12**, which (along with amorphous precipitate) was deposited from the MeCN solution of **Ce-10**. Certainly, rearrangement is necessary given the differences in topology and the differences in the Ce^{IV}:Ce^{III} ratio of **Ce-10** and **Ce-12**.

https://doi.org/10.1021/acs.inorgchem.3c02141
Inorg. Chem. XXXX, XXX, XXX−XXX

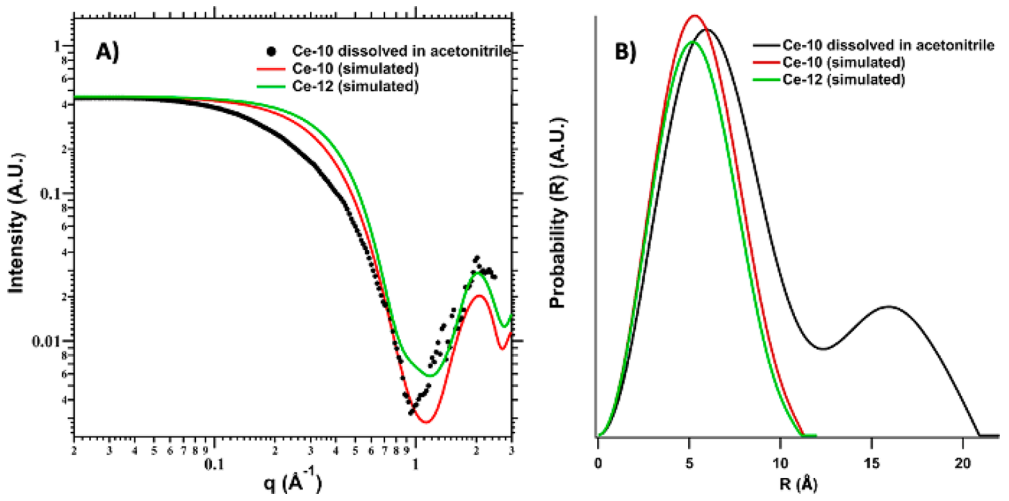

Figure 4. (a) Scattering spectra from **Ce-10** dissolved in acetonitrile, along with simulated scattering for **Ce-10** and **Ce-12**. (b) Pair distance distribution function (PDDF) of the experimental and simulated scattering data.

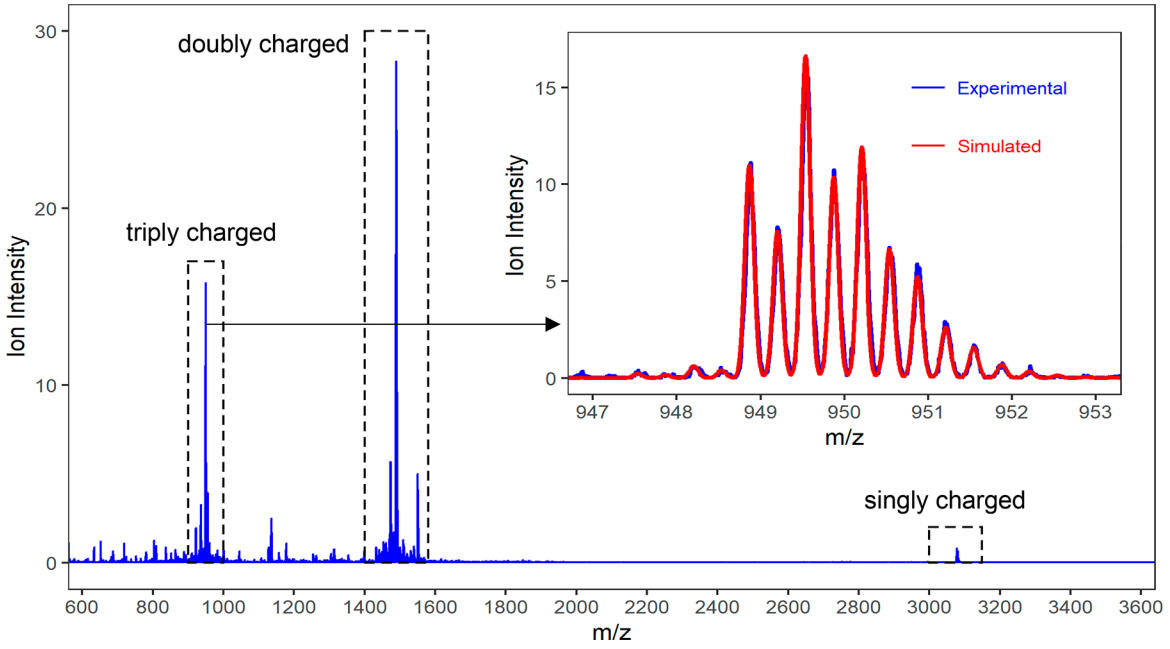

Figure 5. Mass spectra from 600 to 3600 m/z of 50 μM **Ce-10** in a MeCN solution. The boxes with dotted lines highlight the singly, doubly, and triply charged groups of ions. The inset shows the major triply charged ion with a monoisotopic peak at m/z 948.87, with the experimental data from the **Ce-10** solution in blue and the simulated data of **Core Ce-10**(3+) in red.

Comparison of the experimental scattering data for the **Ce-10**/MeCN solution and the simulated scattering for both **Ce-10** and **Ce-12** suggest that **Ce-10** reacts in MeCN to make clusters that are larger than **Ce-10** and **Ce-12**. As shown in Figure 4a, the simulated scattering curves of **Ce-10** and **Ce-12** are similar given the similar size and shape of the clusters. Yet the simulated scattering curve for **Ce-10** suggests a slightly larger size (based on the slight shift to lower q of the Guinier elbow at $q \approx 0.32$ Å^{-1}), despite its smaller nuclearity. In fact, for **Ce-12**, the distance between the periphery Ce^{III} ions is 10.8 Å. On the other hand, comparing the longest Ce−Ce distance within the $\mathbf{Ce_{10}}$ core of **Ce-12** (8.2 Å) to the longest Ce−Ce distance of **Ce-10** (9.3 Å) shows that the **Ce-10** core is actually bigger. This is because the **Ce-10** core contains six Ce^{IV} and four Ce^{III}, while the **Ce-12** core contains ten Ce^{IV}, with commensurate shorter Ce−O bond distances, on average. Clearly there is a mismatch in the Guinier region between the experimental scattering and the simulated scattering for both **Ce-10** and **Ce-12**; the experimental scattering shows a shift to lower q, indicating a larger average size species than both of the crystallized clusters or some aggregation. Fourier transform of the scattering data gives a pair distance distribution function (PDDF) representation (Figures 4b and S19), which is a probability distribution map of scattering vectors through the scattering species, and also provide shape information based on characteristic PDDF profiles.[100]

The PDDFs of the simulated **Ce-10** and **Ce-12** give Gaussian distribution of scattering vectors, as expected for approximately spherical, dense particles, and respective radii of gyration (R_g) of 4.15 and 4.05 Å (Figure S19). R_g is the size-independent, root−mean−squared average of the electrons from the center of the cluster, similar to the radius and related

https://doi.org/10.1021/acs.inorgchem.3c02141
Inorg. Chem. XXXX, XXX, XXX−XXX

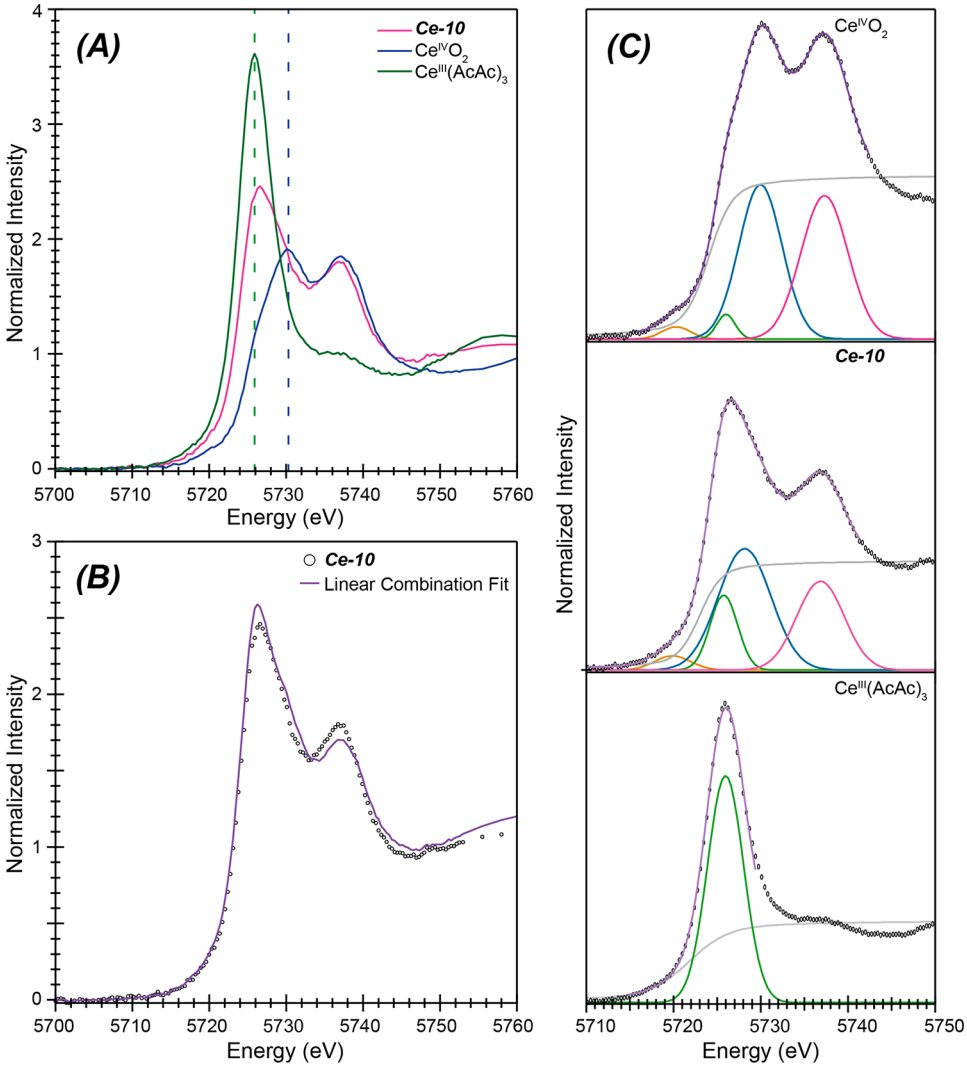

Figure 6. (A) Room temperature background subtracted and normalized Ce L_3-edge XAS spectra (298 K) from **Ce-10** (pink trace). For comparison, spectra collected under analogous conditions from +4 and +3 cerium oxidation state standards were included, namely $Ce^{IV}O_2$ (blue trace) and $Ce^{III}(acac)_3$ (green trace). (B) The normalized Ce L_3-edge spectrum from **Ce-10** (○) and a linear combination analysis fit (purple trace) comprised contributions from the +4 and +3 cerium oxidation state standards, specifically $Ce^{IV}O_2$ and $Ce^{III}(acac)_3$. Contributions from the +4 standard were 56(2)% and contributions from the +3 standard were 44(2)%. (C) Deconvolution of room temperature, background subtracted, and normalized Ce L_3-edge spectra from CeO_2 (top), **Ce-10** (middle), and $Ce(acac)_3$ (bottom). Experimental data (○) were overlaid on the fit (purple trace) and functions used to generate the model. These included Gaussian functions (brown, green, blue, and pink traces) used to model the X-ray absorption peaks and a step function (1:1 combination of an arctangent and error function; gray trace).

by $\sim\sqrt{(5/3)}R_g$ = radius for a spherical particle. The distance (R) where the probability goes to zero is ~11 Å for both **Ce-10** and **Ce-12**, consistent with the longest Ce−O distance within the cluster core. On the other hand, the PDDF for **Ce-10** dissolved in acetonitrile is consistent with the presence of clusters associated as dimers in solution, and an average R_g of 6.9 Å.[100] This sort of association is reminiscent of V_{10} dimerization via H-bonding, observed by SAXS in solution (also observed in the solid state).[101] Because the $acac^{1-}$ ligands are noted to dissociate from the cluster core via ^{1}H NMR in acetonitrile, we suspect the SAXS data indicates that cluster−cluster association in solution is important to the **Ce-10** to **Ce-12** conversion.

Electrospray Ionization Mass Spectrometry (ESI-MS). To further interrogate the identity of the Ce species present in solution upon the dissolution of **Ce-10** in MeCN, ESI-MS data were collected (Figure 5). Ions above 600 m/z were attributed to Ce clusters based on isotopic patterns. Three prominent groups of peaks were observed in the spectrum: peaks around m/z 950, around m/z 1490, and around m/z 3080 corresponded to triply, doubly, and singly charged ions, respectively, based on isotopic pattern spacings. Examination of the ions within these groups showed peaks that were spaced by mass differences corresponding to water and methanol. This was interpreted as the presence of clusters that differed in the number of OH^-, MeO^-, and O^{2-} ligands. To find potential molecular formulas, a combinatorial search was conducted using constraints of 5−15 cerium nuclearity, 7−30 acac ligands, 0−20 OH^- ligands, 0−20 O^{2-} ligands, and 0−20 MeO^- ligands. Only formulas that satisfied the ion charge (based on a combination of Ce^{III} and Ce^{IV}) and were within 30 ppm of the experimental monoisotopic mass were retained.

For the major triply charged ion with monoisotopic peak at m/z 948.87 (Figure 5 inset), the constraints above resulted in 14 formulas, among which 3 were Ce_{11} and 11 were Ce_{10}, indicating more likelihood of Ce_{10} clusters. Moreover, Ce_{11}

https://doi.org/10.1021/acs.inorgchem.3c02141
Inorg. Chem. XXXX, XXX, XXX−XXX

clusters in the original list of 14 had poorer isotopic matching with the experimental data compared to that of Ce_{10} clusters. Further filtering the list using a constraint of 6 Ce^{IV} centers based on crystallographic data resulted in 4 formulas, all of which were Ce_{10} clusters (Table S11). Accordingly, it was concluded that the triply charged ion at m/z 948.8753 represents a Ce_{10} cluster. The inset of Figure 5 depicts isotopic envelope matching between the experimental data and one of the 4 potential formulas: $Ce_{10}(CH_3COCHCOCH_3)_{12}(OH)_5O_7(CH_3O)_2^{3+}$ denoted as **Core Ce-10(3+)**. The doubly and singly charged ion groups in Figure 5 can be interpreted in relation to the triply charged ion at m/z 948.8753 via variations in number of ligands and are further discussed in the Supporting Information (Figures S23–S25).

X-ray Absorption Spectroscopy (XAS). **Ce-10** was examined via Ce L_3-edge X-ray absorption spectroscopy (XAS). Note that limited sample size or impurities precluded similar investigations for **Ce-1** and **Ce-12**. The data were comparatively evaluated against two oxidation state standards: ceria ($Ce^{IV}O_2$) and cerium(III) acetylacetonate [$Ce^{III}(acac)_3$] (Figure 6a). The spectrum from **Ce-10** was hybridic in nature, meaning that it had attributes associated with both oxidation state standard extremes. It showed the double white line characteristic of cerium in a +4 oxidation state. However, the rising edge inflection point 5724.1(1) eV and peak maximum 5726.7(1) eV for the first feature were lower in energy than we expected for a Ce^{IV} complex and suggested Ce^{III}. Another metric for deciphering Ce^{III} vs Ce^{IV} content was the branching ratio between the two absorption features of the double white line peak: $\left(\frac{\textit{Low Energy Feature Intensity}}{\textit{Low Energy Feature Intensity} + \textit{High Energy Feature Intensity}}\right)$.[24,102−106] The +4 oxidation state standard, $Ce^{IV}O_2$, had a branching ratio of 0.51. In contrast, the double white line branching ratio (determined via curve fitting analysis) for **Ce-10** was 0.67. The high branching ratio in **Ce-10** reflected that the low energy absorption feature was substantially more intense than the high energy feature. Higher branching ratios can be indicative of compounds that contain both Ce^{III} and Ce^{IV}, which was consequently how we interpreted this spectrum.[107]

In **Ce-10**, there are eight oxo dianions, 14 $acac^{1-}$ monoanions, and six methoxide ligands; the total number of negative charges is 36. The presence of a double white line absorption feature in the Ce L_3-edge X-ray absorption spectrum unambiguously refuted homovalent Ce^{III} models of the spectrum. It was also difficult to rationalize that the XAS data could originate from a cluster that only had Ce^{IV} cations because of (1) the low energy associated with the rising edge inflection point, (2) the low energy for the first peak maximum, and (3) the relative intensities from the two features (high branching ratio). Instead, the experiments suggested that two contributions to the Ce_{10} XAS spectrum existed: one from cerium in the +3 oxidation state and another from cerium in the +4 oxidation state. Under the aforementioned designation (with six methoxide ligands), there was one way to charge balance and generate a neutral cluster: four Ce^{III} and six Ce^{IV}. We fit the data from **Ce-10** as a summation of spectra from the two oxidation state standards to test the validity of this description. This was achieved using the following equation:

$$Fit = N \times Ce(acac)_{3(spectrum)} + (1 - N) \times CeO_{2(spectrum)}$$

Here, $Ce(acac)_{3(spectrum)}$ was the L_3-edge XAS data from $Ce(acac)_3$, $CeO_{2(spectrum)}$ was the L_3-edge XAS data from CeO_2, and N was a linear combination mixing coefficient. The resulting model fit excellently the features, relative intensities, and overall line shape of the Ce L_3-edge XAS data from **Ce-10** (R-factor = 3.6%). The model consisted of a 44(2)% contribution from the +3 standard [$Ce(acac)_3$] and 56(2)% contribution from the +4 standard CeO_2 (Figure 6b). These experimentally determined +3 vs +4 contribution values were equivalent to the charge balanced description of **Ce-10** mentioned above and the bond valence summation values from the structural analysis: four Ce^{III} cations and six Ce^{IV} cations.

CONCLUSION

A discrete Ce-oxo cluster, $Ce_{10}O_8(acac)_{14}(CH_3O)_6(CH_3OH)_2]\cdot 10.5$ MeOH (**Ce-10**), and a monomeric molecule, $Ce(acac)_4$, were isolated from methanol and ethanol solutions, respectively. Dissolution of **Ce-10** in acetonitrile led to the isolation of another discrete Ce-oxo cluster, $[Ce_{12}O_{12}(OH)_4(acac)_{16}(CH_3COO)_2]\cdot(MeCN)_6$ (**Ce-12**). Bond valence summation performed for both clusters showed Ce^{III}/Ce^{IV} mixed oxidation state cluster cores, with XAS data confirming this assignment for the Ce-10 cluster. The stability of **Ce-10** in solution was probed using SAXS and ESI-MS. The ESI-MS exhibits peaks consistent with decanuclear (Ce_{10}) species. SAXS identifies the presence of clusters in solution (either **Ce-10** and/or **Ce-12**) that are associated via dispersive or hydrophobic interactions, which may be important for the conversion of **Ce-10** to **Ce-12**. Overall, this study points to the utility of β-diketonate ligand scaffolds in stabilizing novel cluster cores and the role that solvent identity has on cluster formation. Note, in methanol, we isolated methoxy bridged polynuclear species, and in ethanol, we isolated monomeric structural units. Given ongoing interest in Ce-oxo cluster chemistry in catalysis application spaces and for advancing fundamental insight into lanthanide and actinide oxo cluster chemistry, our ongoing efforts center on identifying solution stable species and probing their chemical reactivity and catalytic behavior. Additionally, we are excited about the prospect of extending these results to actinide systems and characterizing similarities and/or differences between Ce and Pu cluster chemistry.

ASSOCIATED CONTENT

Supporting Information

The Supporting Information is available free of charge at https://pubs.acs.org/doi/10.1021/acs.inorgchem.3c02141.

Crystallographic refinement details, thermal ellipsoid plots, packing diagrams for **Ce-1**, **Ce-10**, and **Ce-12**, descriptions of Ce coordination chemistry in **Ce-10** and **Ce-12**, powder X-ray diffraction patterns, small-angle X-ray scattering PDDF, IR and NMR spectra, bond valence summation values, XAS sample preparation, instrument configuration, data analysis, summary of previously reported homometallic cerium-oxo clusters (PDF)

Accession Codes

CCDC 2257002−2257006 contain the supplementary crystallographic data for this paper. These data can be obtained free of charge via www.ccdc.cam.ac.uk/data_request/cif, or by emailing data_request@ccdc.cam.ac.uk, or by contacting The

https://doi.org/10.1021/acs.inorgchem.3c02141
Inorg. Chem. XXXX, XXX, XXX−XXX

Cambridge Crystallographic Data Centre, 12 Union Road, Cambridge CB2 1EZ, UK; fax: + 44 1223 336033.

AUTHOR INFORMATION

Corresponding Author

Karah E. Knope − *Department of Chemistry, Georgetown University, Washington, D.C. 20057, United States;* orcid.org/0000-0002-5690-715X; Email: kek44@georgetown.edu

Authors

Anamar Blanes-Díaz − *Department of Chemistry, Georgetown University, Washington, D.C. 20057, United States*

Mohammad Shohel − *Department of Chemistry, Oregon State University, Corvallis, Oregon 97331, United States*

Natalie T. Rice − *Los Alamos National Laboratory (LANL), Los Alamos, New Mexico 87545, United States*

Ida Piedmonte − *Los Alamos National Laboratory (LANL), Los Alamos, New Mexico 87545, United States*

Morgan A. McDonald − *Department of Chemistry, Georgetown University, Washington, D.C. 20057, United States;* orcid.org/0009-0008-5452-4463

Kaveh Jorabchi − *Department of Chemistry, Georgetown University, Washington, D.C. 20057, United States;* orcid.org/0000-0003-2569-4048

Stosh A. Kozimor − *Los Alamos National Laboratory (LANL), Los Alamos, New Mexico 87545, United States;* orcid.org/0000-0001-7387-0507

Jeffery A. Bertke − *Department of Chemistry, Georgetown University, Washington, D.C. 20057, United States;* orcid.org/0000-0002-3419-5163

May Nyman − *Department of Chemistry, Oregon State University, Corvallis, Oregon 97331, United States;* orcid.org/0000-0002-1787-0518

Complete contact information is available at: https://pubs.acs.org/10.1021/acs.inorgchem.3c02141

Author Contributions

The manuscript was written through contributions of all authors. All authors have given approval to the final version of the manuscript.

Notes

The authors declare no competing financial interest.

ACKNOWLEDGMENTS

This work was primarily supported by the U.S. Department of Energy, Office of Science, Office of Basic Energy Sciences, Early Career Research Program under Award DE-SC0019190. KEK, MAM, and KJ also acknowledge support from the Georgetown University Earth Commons, EcoImpact Award. SAXS data were collected and analyzed at OSU; SM and MN are supported by the U.S. Department of Energy, National Nuclear Security Administration under Award DE-NA0003763. For XAS measurements, SAK, NTR, and IDP acknowledge the U.S. Department of Energy, Office of Science, Office of Basic Energy Sciences, Heavy Element Chemistry program (LANLE372) and LANL's LDRD−DR project (20220054DR). In addition, SAK, NTR, and IDP are grateful to the LANL Directors Post-Doctoral Fellowship program (NTR) and the Agnew Postdoctoral Fellowship program (IDP) for support. Los Alamos National Laboratory is operated by Triad National Security, LLC, for the National Nuclear Security Administration of U.S. Department of Energy (Contract No. 89233218CNA000001).

REFERENCES

(1) Liu, Y.; Li, Y.; He, X. In situ synthesis of ceria nanoparticles in the ordered mesoporous carbon as a novel electrochemical sensor for the determination of hydrazine. *Anal. Chim. Acta* **2014**, *819*, 26−33.

(2) Hu, J.; Ren, S.; Witter, R.; Fichtner, M. Catalytic Influence of Various Cerium Precursors on the Hydrogen Sorption Properties of $NaAlH_4$. *Adv. Energy Mater.* **2012**, *2* (5), 560−568.

(3) Bhushan, B.; Nandhagopal, S.; Rajesh Kannan, R.; Gopinath, P. Biomimetic nanomaterials: Development of protein coated nanoceria as a potential antioxidative nano-agent for the effective scavenging of reactive oxygen species in vitro and in zebrafish model. *Colloids Surf., B* **2016**, *146*, 375−86.

(4) Qiao, Y.; Sergentu, D. C.; Yin, H.; Zabula, A. V.; Cheisson, T.; McSkimming, A.; Manor, B. C.; Carroll, P. J.; Anna, J. M.; Autschbach, J.; Schelter, E. J. Understanding and Controlling the Emission Brightness and Color of Molecular Cerium Luminophores. *J. Am. Chem. Soc.* **2018**, *140* (13), 4588−4595.

(5) Wang, X.; Brunson, K.; Xie, H.; Colliard, I.; Wasson, M. C.; Gong, X.; Ma, K.; Wu, Y.; Son, F. A.; Idrees, K. B.; Zhang, X.; Notestein, J. M.; Nyman, M.; Farha, O. K. Heterometallic Ce^{IV}/ V^{V} Oxo Clusters with Adjustable Catalytic Reactivities. *J. Am. Chem. Soc.* **2021**, *143* (49), 21056−21065.

(6) Wasson, M. C.; Zhang, X.; Otake, K.-i.; Rosen, A. S.; Alayoglu, S.; Krzyaniak, M. D.; Chen, Z.; Redfern, L. R.; Robison, L.; Son, F. A.; Chen, Y.; Islamoglu, T.; Notestein, J. M.; Snurr, R. Q.; Wasielewski, M. R.; Farha, O. K. Supramolecular Porous Assemblies of Atomically Precise Catalytically Active Cerium-Based Clusters. *Chem. Mater.* **2020**, *32* (19), 8522−8529.

(7) Janoš, P.; Ederer, J.; Pilařová, V.; Henych, J.; Tolasz, J.; Milde, D.; Opletal, T. Chemical mechanical glass polishing with cerium oxide: Effect of selected physico-chemical characteristics on polishing efficiency. *Wear* **2016**, *362*−*363*, 114−120.

(8) Kašpar, J.; Fornasiero, P.; Graziani, M. Use of CeO_2-based oxides in the three-way catalysis. *Catal. Today* **1999**, *50* (2), 285−298.

(9) Flytzani-Stephanopoulos, M. Nanostructured Cerium Oxide "Ecocatalysts. *MRS Bull.* **2001**, *26* (11), 885−889.

(10) Schelter, E. J. Cerium under the lens. *Nat. Chem.* **2013**, *5* (4), 348.

(11) Bogart, J. A.; Lippincott, C. A.; Carroll, P. J.; Booth, C. H.; Schelter, E. J. Controlled Redox Chemistry at Cerium within a Tripodal Nitroxide Ligand Framework. *Chemistry* **2015**, *21* (49), 17850−9.

(12) Gao, P.; Kang, Z.; Fu, W.; Wang, W.; Bai, X.; Wang, E. Electrically Driven Redox Process in Cerium Oxides. *J. Am. Chem. Soc.* **2010**, *132*, 4197−4201.

(13) Lv, X.; Zhao, X. L.; Zhao, Q.; Zheng, Q.; Xuan, W. Cerium-oxo clusters for photocatalytic aerobic oxygenation of sulfides to sulfoxides. *Dalton Trans.* **2022**, *51* (23), 8949−8954.

(14) Mitchell, K. J.; Goodsell, J. L.; Russell-Webster, B.; Twahir, U. T.; Angerhofer, A.; Abboud, K. A.; Christou, G. Expansion of the Family of Molecular Nanoparticles of Cerium Dioxide and Their Catalytic Scavenging of Hydroxyl Radicals. *Inorg. Chem.* **2021**, *60* (3), 1641−1653.

(15) Duval, S.; Béghin, S.; Falaise, C.; Trivelli, X.; Rabu, P.; Loiseau, T. Stabilization of Tetravalent 4f (Ce), 5d (Hf), or 5f (Th, U) Clusters by the $[\alpha\text{-}SiW_9O_{34}]^{10-}$ Polyoxometalate. *Inorg. Chem.* **2015**, *54* (17), 8271−8280.

(16) Guillou, N.; Auffrédic, J. P.; Louër, D. Synthesis, Crystal Structure, and Thermal Behavior of Cerium(IV) Oxide Nitrate $Ce_2O(NO_3)_6(H_2O)_6 \cdot 2H_2O$. *J. Solid State Chem.* **1994**, *112*, 45−52.

(17) Hennig, C.; Ikeda-Ohno, A.; Kraus, W.; Weiss, S.; Pattison, P.; Emerich, H.; Abdala, P. M.; Scheinost, A. C. Crystal Structure and Solution Species of Ce(III) and Ce(IV) Formates: From Mononuclear to Hexanuclear Complexes. *Inorg. Chem.* **2013**, *52* (20), 11734−11743.

(18) Russell-Webster, B.; Lopez-Nieto, J.; Abboud, K. A.; Christou, G. Truly Monodisperse Molecular Nanoparticles of Cerium Dioxide of 2.4 nm dimensions: A $\{Ce_{100}O_{167}\}$ Cluster. *Angew. Chem., Int. Ed. Engl.* **2021**, *60* (22), 12591−12596.
(19) Ma, P.; Wan, R.; Wang, Y.; Hu, F.; Zhang, D.; Niu, J.; Wang, J. Coordination-Driven Self-Assembly of a 2D Graphite-Like Framework Constructed from High-Nuclear Ce_{10} Cluster Encapsulated Polyoxotungstates. *Inorg. Chem.* **2016**, *55* (2), 918−924.
(20) Malaestean, I. L.; Ellern, A.; Baca, S.; Kogerler, P. Cerium oxide nanoclusters: commensurate with concepts of polyoxometalate chemistry? *Chem. Commun.* **2012**, *48* (10), 1499−501.
(21) Mitchell, K. J.; Abboud, K. A.; Christou, G. Atomically-precise colloidal nanoparticles of cerium dioxide. *Nat. Commun.* **2017**, *8* (1), 1445.
(22) Smolders, S.; Struyf, A.; Reinsch, H.; Bueken, B.; Rhauderwiek, T.; Mintrop, L.; Kurz, P.; Stock, N.; De Vos, D. E. A precursor method for the synthesis of new Ce(IV) MOFs with reactive tetracarboxylate linkers. *ChemComm* **2018**, *54* (8), 876−879.
(23) Russell-Webster, B.; Abboud, K. A.; Christou, G. Molecular nanoparticles of cerium dioxide: structure-directing effect of halide ions. *ChemComm* **2020**, *56* (40), 5382−5385.
(24) Wacker, J. N.; Ditter, A. S.; Cary, S. K.; Murray, A. V.; Bertke, J. A.; Seidler, G. T.; Kozimor, S. A.; Knope, K. E. Reactivity of a Chloride Decorated, Mixed Valent $Ce^{III/IV38}$-Oxo Cluster. *Inorg. Chem.* **2022**, *61* (1), 193−205.
(25) Estes, S. L.; Antonio, M. R.; Soderholm, L. Tetravalent Ce in the Nitrate-Decorated Hexanuclear Cluster $[Ce_6(\mu_3\text{-}O)_4(\mu_3\text{-}OH)_4]^{12+}$: A Structural End Point for Ceria Nanoparticles. *J. Phys. Chem. C* **2016**, *120* (10), 5810−5818.
(26) Gibbs, F. E.; Olson, D. L.; Hutchinson, W. Identification of a Physical Metallurgy Surrogate for the Plutonium- 1 wt.% Gallium Alloy. *Plutonium Futures - The Science: Topical Conference on Plutonium and Actinides* **2000**, *532*, 98−101.
(27) Koelling, D. D. Cerium Compounds in the Fashion of the Light Actinides. *Physica B+C* **1985**, *130*, 135.
(28) Klamm, B. E.; Windorff, C. J.; Marsh, M. L.; Meeker, D. S.; Albrecht-Schmitt, T. E. Schiff-base coordination complexes with plutonium(IV) and cerium(IV). *Chem. Commun.* **2018**, *54* (62), 8634−8636.
(29) Shannon, R. D.; Prewitt, C. T. Effective ionic radii in oxides and fluorides. *Acta Crystallogr.* **1969**, *25* (5), 925−946.
(30) Wadsworth, E.; Duke, F. R.; Goetz, C. A. Present Status of Cerium(IV)-Cerium(III) Potentials. *Anal. Chem.* **1957**, *29* (12), 1824−1825.
(31) Kim, S.-Y.; Asakura, T.; Morita, Y. *Electrochemical studies of plutonium(IV) complexes in aqueous nitrate solutions*; Japan, 2005; pp 341−344.
(32) Xu, J.; Radkov, E.; Ziegler, M.; Raymond, K. N. Plutonium(IV) Sequestration: Structural and Thermodynamic Evaluation of the Extraordinarily Stable Cerium(IV) Hydroxypyridinonate Complexes1. *Inorg. Chem.* **2000**, *39* (18), 4156−4164.
(33) Sigmon, G. E.; Hixon, A. E. Extension of the Plutonium Oxide Nanocluster Family to Include Pu(16) and Pu(22). *Chem. Eur. J.* **2019**, *25* (10), 2463−2466.
(34) Soderholm, L.; Almond, P. M.; Skanthakumar, S.; Wilson, R. E.; Burns, P. C. The structure of the plutonium oxide nanocluster $[Pu_{38}O_{56}Cl_{54}(H_2O)_8]^{14-}$. *Angew. Chem., Int. Ed. Engl.* **2008**, *47* (2), 298−302.
(35) Knope, K. E.; Soderholm, L. Plutonium(IV) cluster with a hexanuclear $[Pu_6(OH)_4O_4]^{12+}$ core. *Inorg. Chem.* **2013**, *52* (12), 6770−2.
(36) Novikov, A. P.; Kalmykov, S. N.; Utsunomiya, S.; Ewing, R. C.; Horreard, F.; Merkulov, A.; Clark, S. B.; Tkachev, V. V.; Myasoedov, B. F. Colloid Transport of Plutonium in the Far-Field of the Mayak Production Association, Russia. *Science* **2006**, *314* (5799), 638−641.
(37) Kersting, A. B.; Zavarin, M. Colloid-Facilitated Transport of Plutonium at the Nevada Test Site, NV, USA. *In Actinide Nanoparticle Research* **2011**, 399−412.
(38) Clark, D. L.; Janecky, D. R.; Lane, L. J. Science-based cleanup of Rocky Flats. *Phys. Today* **2006**, *59* (9), 34−40.
(39) Gerber, E.; Romanchuk, A. Y.; Weiss, S.; Kuzenkova, A.; Hunault, M.; Bauters, S.; Egorov, A.; Butorin, S. M.; Kalmykov, S. N.; Kvashnina, K. O. To form or not to form: PuO_2 nanoparticles at acidic pH. *Environ. Sci. Nano.* **2022**, *9* (4), 1509−1518.
(40) Petit, S.; Baril-Robert, F.; Pilet, G.; Reber, C.; Luneau, D. Luminescence spectroscopy of europium(III) and terbium(III) penta-, octa- and nonanuclear clusters with beta-diketonate ligands. *Dalton Trans.* **2009**, No. 34, 6809−15.
(41) Wang, W.-M.; Xue, C.-L.; Jing, R.-Y.; Ma, X.; Yang, L.-N.; Luo, S.-C.; Wu, Z.-L. Two hexanuclear lanthanide Ln_6^{III} clusters featuring remarkable magnetocaloric effect and slow magnetic relaxation behavior. *New J. Chem.* **2020**, *44* (41), 18025−18030.
(42) Brese, N. E.; O'Keeffe, M. Bond-Valence Parameters for Solids. *Acta Crystallogr.* **1991**, *B47*, 192−197.
(43) Brown, I. D. Recent Developments in the Methods and Applications of the Bond Valence Model. *Chem. Rev.* **2009**, *109*, 6858−6919.
(44) *SAINT*; Bruker AXS Inc: Madison, WI, 2007.
(45) *APEX3*; Bruker AXS Inc: Madison, WI, 2016.
(46) *SADABS*; Bruker AXS Inc.: Madison, WI, 2008.
(47) Hubschle, C. B.; Sheldrick, G. M.; Dittrich, B. ShelXle: a Qt graphical user interface for SHELXL. *J. Appl. Crystallogr.* **2011**, *44* (6), 1281−1284.
(48) Sheldrick, G. A short history of SHELX. *Acta Crystallogr., Sect. A* **2008**, *64* (1), 112−122.
(49) Jahrman, E. P.; Holden, W. M.; Ditter, A. S.; Mortensen, D. R.; Seidler, G. T.; Fister, T. T.; Kozimor, S. A.; Piper, L. F. J.; Rana, J.; Hyatt, N. C.; Stennett, M. C. An improved laboratory-based x-ray absorption fine structure and x-ray emission spectrometer for analytical applications in materials chemistry research. *Rev. Sci. Instrum.* **2019**, *90* (2), 024106.
(50) Solomon, E. I.; Hedman, B.; Hodgson, K. O.; Dey, A.; Szilagyi, R. K. Ligand K-edge X-ray absorption spectroscopy: covalency of ligand-metal bonds. *Coord. Chem. Rev.* **2005**, *249* (1), 97−129.
(51) Ilavsky, J.; Jemian, P. R. Irena: tool suite for modeling and analysis of small-angle scattering. *J. Appl. Crystallogr.* **2009**, *42* (2), 347−353.
(52) Zuo, X.; Cui, G.; Merz, K. M.; Zhang, L.; Lewis, F. D.; Tiede, D. M. X-ray diffraction "fingerprinting"of DNA structure in solution for quantitative evaluation of molecular dynamics simulation. *Proc. Natl. Acad. Sci. U. S. A.* **2006**, *103* (10), 3534−3539.
(53) Matkovic, B.; Grdenic, D. The Crystal Structure of Cerium(IV) Acetylacetonate. *Acta Crystallogr.* **1963**, *16*, 456−461.
(54) Brown, I. D. *Bond Valence Parameters*; International Union of Crystallography, 2020. https://www.iucr.org/resources/data/datasets/bond-valence-parameters (accessed 08-14-2023).
(55) Albat, M.; Stock, N. Multiparameter High-Throughput and in Situ X-ray Diffraction Study of Six New Bismuth Sulfonatocarboxylates: Discovery, Phase Transformation, and Reaction Trends. *Inorg. Chem.* **2018**, *57* (16), 10352−10363.
(56) Loera Fernandez, I. I.; Donaldson, S. L.; Schipper, D. E.; Andleeb, S.; Whitmire, K. H. Anionic Bismuth-Oxido Carboxylate Clusters with Transition Metal Countercations. *Inorg. Chem.* **2016**, *55* (21), 11560−11569.
(57) Miersch, L.; Rüffer, T.; Lang, H.; Schulze, S.; Hietschold, M.; Zahn, D.; Mehring, M. A Novel Water-Soluble Hexanuclear Bismuth Oxido Cluster - Synthesis, Structure and Complexation with Polyacrylate. *EurJIC* **2010**, *2010* (30), 4763−4769.
(58) Miersch, L.; Ruffer, T.; Schlesinger, M.; Lang, H.; Mehring, M. Hydrolysis studies on bismuth nitrate: synthesis and crystallization of four novel polynuclear basic bismuth nitrates. *Inorg. Chem.* **2012**, *51* (17), 9376−84.
(59) Senevirathna, D. C.; Werrett, M. V.; Blair, V. L.; Mehring, M.; Andrews, P. C. 2D and 3D Coordination Networks of Polynuclear Bismuth Oxido/Hydroxido Sulfonato Clusters from Low Temperature Solid-State Metathesis Reactions. *Chem. Eur. J.* **2018**, *24* (26), 6722−6726.

https://doi.org/10.1021/acs.inorgchem.3c02141
Inorg. Chem. XXXX, XXX, XXX−XXX

(60) Yuan, S.; Qin, J. S.; Li, J.; Huang, L.; Feng, L.; Fang, Y.; Lollar, C.; Pang, J.; Zhang, L.; Sun, D.; Alsalme, A.; Cagin, T.; Zhou, H. C. Retrosynthesis of multi-component metal-organic frameworks. *Nat. Commun.* **2018**, *9* (1), 808.
(61) Deria, P.; Gomez-Gualdron, D. A.; Bury, W.; Schaef, H. T.; Wang, T. C.; Thallapally, P. K.; Sarjeant, A. A.; Snurr, R. Q.; Hupp, J. T.; Farha, O. K. Ultraporous, Water Stable, and Breathing Zirconium-Based Metal-Organic Frameworks with ftw Topology. *J. Am. Chem. Soc.* **2015**, *137* (40), 13183−90.
(62) Kickelbick, G.; Puchberger, M.; Schubert, U.; Gross, S. Mono-, Di-, and Trimetallic Methacrylate-substituted Metal Oxide Clusters Derived from Hafnium Butoxide. *Monatsh. Chem.* **2003**, *134* (8), 1053−1063.
(63) Poschmann, M. P. M.; Waitschat, S.; Reinsch, H.; Stock, N. Synthesis of two new Hf-MOFs with UiO-66 and CAU-22 structure employing 2,5-pyrazinedicarboxylic acid as linker molecule. *Z. Anorg. Allg. Chem.* **2021**, *647* (22), 2029−2034.
(64) Matsuoka, M.; Tsushima, S.; Takao, K. Fluorite-like hydrolyzed hexanuclear coordination clusters of Zr(IV) and Hf(IV) with syn-syn bridging N,N,N-trimethylglycine in soft crystal structures exhibiting cold-crystallization. *Inorg. Chim. Acta* **2021**, *528*, 120622.
(65) Knope, K. E.; Wilson, R. E.; Vasiliu, M.; Dixon, D. A.; Soderholm, L. Thorium(IV) molecular clusters with a hexanuclear Th core. *Inorg. Chem.* **2011**, *50* (19), 9696−704.
(66) Li, Z. J.; Ju, Y.; Zhang, Z.; Lu, H.; Li, Y.; Zhang, N.; Du, X. L.; Guo, X.; Zhang, Z. H.; Qian, Y.; He, M. Y.; Wang, J. Q.; Lin, J. Unveiling the Unique Roles of Metal Coordination and Modulator in the Polymorphism Control of Metal-Organic Frameworks. *Chem. Eur. J.* **2021**, *27* (70), 17586−17594.
(67) Lu, H.; Xu, M.; Zheng, Z.; Liu, Q.; Qian, J.; Zhang, Z. H.; He, M. Y.; Qian, Y.; Wang, J. Q.; Lin, J. Emergence of Thorium-Based Polyoxo Clusters as a Platform for Selective X-ray Dosimetry. *Inorg. Chem.* **2021**, *60* (24), 18629−18633.
(68) Berthet, J. C.; Thuery, P.; Ephritikhine, M. Formation of uranium(IV) oxide clusters from uranocene $[U(n^8\text{-}C_8H_8)_2]$ and uranyl $[UO_2X_2]$ compounds. *Inorg. Chem.* **2010**, *49* (17), 8173−7.
(69) Vanagas, N. A.; Higgins, R. F.; Wacker, J. N.; Asuigui, D. R. C.; Warzecha, E.; Kozimor, S. A.; Stoll, S. L.; Schelter, E. J.; Bertke, J. A.; Knope, K. E. Mononuclear to Polynuclear U^{IV} Structural Units: Effects of Reaction Conditions on U-Furoate Phase Formation. *Chem. Eur. J.* **2020**, *26* (26), 5872−5886.
(70) Knope, K. E.; Soderholm, L. Solution and solid-state structural chemistry of actinide hydrates and their hydrolysis and condensation products. *Chem. Rev.* **2013**, *113* (2), 944−94.
(71) Nolan, M.; Parker, S. C.; Watson, G. W. The electronic structure of oxygen vacancy defects at the low index surfaces of ceria. *Surf. Sci.* **2005**, *595* (1−3), 223−232.
(72) Yuan, Y.; Ji, X.; Zhao, D. Efficient Oxidative Cleavage of 1,3-Dicarbonyl Derivatives with Hydrogen Peroxide Catalyzed by Quaternary Ammonium Iodide. *EurJOC* **2010**, *2010* (27), 5274−5278.
(73) Boyle, T. J.; Tribby, L. J.; Bunge, S. D. Synthesis and Structural Characterization of a Series of Carboxylic Acid Modified Cerium(III) Alkoxides. *EurJIC* **2006**, *2006* (22), 4553−4563.
(74) Bilyk, A.; Dunlop, J. W.; Fuller, R. O.; Hall, A. K.; Harrowfield, J. M.; Hosseini, M. W.; Koutsantonis, G. A.; Murray, I. W.; Skelton, B. W.; Sobolev, A. N.; Stamps, R. L.; White, A. H. Systematic Structural Coordination Chemistry of p-tert-Butyltetrathiacalix[4]arene: Further Complexes of Lanthanide Metal Ions. *EurJIC* **2010**, *2010* (14), 2127−2152.
(75) Aspinall, H. C.; Bacsa, J.; Jones, A. C.; Wrench, J. S.; Black, K.; Chalker, P. R.; King, P. J.; Marshall, P.; Werner, M.; Davies, H. O.; Odedra, R. Ce(IV) Complexes with Donor-Functionalized Alkoxide Ligands: Improved Precursors for Chemical Vapor Deposition of CeO2. *Inorg. Chem.* **2011**, *50* (22), 11644−11652.
(76) Baisch, U.; Dell' Amico, D. B.; Calderazzo, F.; Labella, L.; Marchetti, F.; Vitali, D. Reaction of a tetranuclear N,N-di-iso-propylcarbamato complex of cerium(III) with dioxygen: synthesis and X-ray characterization of both the oxidation product and its precursor. *J. Mol. Catal. A Chem.* **2003**, *204*−*205*, 259−265.
(77) Russell-Webster, B.; Lopez-Nieto, J.; Abboud, K. A.; Christou, G. Phosphorus-based ligand effects on the structure and radical scavenging ability of molecular nanoparticles of CeO2. *Dalton Trans.* **2021**, *50* (43), 15524−15532.
(78) Norton, K.; Banerjee, S.; Das, S.; Huebner, L.; Emge, T. J.; Brennan, J. G. Lanthanide oxochalcogenido clusters. *Dalton Trans.* **2010**, *39* (29), 6794−6800.
(79) Mathey, L.; Paul, M.; Coperet, C.; Tsurugi, H.; Mashima, K. Cerium(IV) Hexanuclear Clusters from Cerium(III) Precursors: Molecular Models for Oxidative Growth of Ceria Nanoparticles. *Chem. Eur. J.* **2015**, *21* (38), 13454−61.
(80) Tamain, C.; Dumas, T.; Hennig, C.; Guilbaud, P. Coordination of Tetravalent Actinides (An = Th^{IV}, U^{IV}, Np^{IV}, Pu^{IV}) with DOTA: From Dimers to Hexamers. *Chem. Eur. J.* **2017**, *23* (28), 6864−6875.
(81) Duval, S.; Roussel, P.; Loiseau, T. Synthesis of a large dodecameric cerium cluster stabilized by the $[SiW_9O_{34}]^{10-}$ polyoxometalate. *Inorg. Chem. Commun.* **2017**, *83*, 52−54.
(82) Mattausch, H.; Kienle, L.; Duppel, V.; Hoch, C.; Simon, A. Seltenerdethenidhalogenide$Ln_{2n+6}(C_2)_{n+4}X_{2n+2}$: Darstellung, Struktur, Verwachsung und Verzwilligung. *Z. Anorg. Allg. Chem.* **2009**, *635* (11), 1527−1535.
(83) Malaestean, I. L.; Ellern, A.; Kögerler, P. $\{Ce_{10}Mn_8\}$: Cerium Analogues of the Decavanadate Archetype. *EurJIC* **2013**, *2013* (10−11), 1635−1638.
(84) Groom, C. R.; Bruno, I. J.; Lightfoot, M. P.; Ward, S. C. The Cambridge Structural Database. *Acta Crystallogr.* **2016**, *B72*, 171−179.
(85) Ling, J.; Lu, H.; Wang, Y.; Johnson, K.; Wang, S. One-dimensional chain structures of hexanuclear uranium(iv) clusters bridged by formate ligands. *RSC Adv.* **2018**, *8* (61), 34947−34953.
(86) Biswas, B.; Mougel, V.; Pecaut, J.; Mazzanti, M. Base-driven assembly of large uranium oxo/hydroxo clusters. *Angew. Chem., Int. Ed. Engl.* **2011**, *50* (25), 5745−8.
(87) Ryazanov, M.; Mattausch, H.; Simon, A. The extended chain compounds $Ln_{12}(C_2)_3I_{17}$ (Ln = Pr, Nd, Gd, Dy): Synthesis, structure and physical properties. *J. Solid State Chem.* **2007**, *180* (4), 1372−1380.
(88) Han, Y.; Li, X.; Li, L.; Ma, C.; Shen, Z.; Song, Y.; You, X. Structures and Properties of Porous Coordination Polymers Based on Lanthanide Carboxylate Building Units. *Inorg. Chem.* **2010**, *49* (23), 10781−10787.
(89) Zhang, Z.-M.; Zangana, K. H.; Kostopoulos, A. K.; Tong, M.-L.; Winpenny, R. E. P. A pseudo-icosahedral cage $\{Gd_{12}\}$ based on aminomethylphosphonate. *Dalton Trans.* **2016**, *45* (22), 9041−9044.
(90) Langley, S. K.; Moubaraki, B.; Tomasi, C.; Evangelisti, M.; Brechin, E. K.; Murray, K. S. Synthesis, Structure, and Magnetism of a Family of Heterometallic $\{Cu_2Ln_7\}$ and $\{Cu_4Ln_{12}\}$ (Ln = Gd, Tb, and Dy) Complexes: The Gd Analogues Exhibiting a Large Magneto-caloric Effect. *Inorg. Chem.* **2014**, *53* (24), 13154−13161.
(91) Miao, Y.-L.; Liu, J.-L.; Leng, J.-D.; Lin, Z.-J.; Tong, M.-L. Chloride templated formation of $\{Dy_{12}(OH)_{16}\}^{20+}$ cluster core incorporating 1,10-phenanthroline-2,9-dicarboxylate. *CrystEngComm* **2011**, *13* (10), 3345−3348.
(92) Mattausch, H.; Hoch, C.; Simon, A. Crystal structure of dodecacerium heptadecaiodide triethanide, $Ce_{12}I_{17}(C_2)_3$. *Z.Kristallogr.-New Cryst.Struct.* **2005**, *220*, 301.
(93) Das Gupta, S.; Thuijs, A. E.; Fisher, E. G.; Abboud, K. A.; Christou, G. $Mn^{II/III}$ and $Ce^{III/IV}$ Units Supported on an Octahedral Molecular Nanoparticle of CeO_2. *Inorg. Chem.* **2022**, *61* (17), 6392−6402.
(94) Thuijs, A. E.; Li, X. G.; Wang, Y. P.; Abboud, K. A.; Zhang, X. G.; Cheng, H. P.; Christou, G. Molecular analogue of the perovskite repeating unit and evidence for direct Mn^{III}-Ce^{IV}-Mn^{III} exchange coupling pathway. *Nat. Commun.* **2017**, *8* (1), 500.
(95) McIver, R. T.; Scott, J. A.; Riveros, J. M. Effect of solvation on the instrinsic relative acidity of methanol and ethanol. *J. Am. Chem. Soc.* **1973**, *95* (8), 2706−2708.

https://doi.org/10.1021/acs.inorgchem.3c02141
Inorg. Chem. XXXX, XXX, XXX−XXX

(96) Wattanathana, W.; Suetrong, N.; Kongsamai, P.; Chansaenpak, K.; Chuanopparat, N.; Hanlumyuang, Y.; Kanjanaboos, P.; Wannapaiboon, S. Crystallographic and Spectroscopic Investigations on Oxidative Coordination in the Heteroleptic Mononuclear Complex of Cerium and Benzoxazine Dimer. *Molecules* **2021**, *26* (17), 5410.
(97) Behrsing, T.; Bond, A. M.; Deacon, G. B.; Forsyth, C. M.; Forsyth, M.; Kamble, K. J.; Skelton, B. W.; White, A. H. Cerium acetylacetonates—new aspects, including the lamellar clathrate $[Ce(acac)_4]\cdot 10H_2O$. *Inorg. Chim. Acta* **2003**, *352*, 229−237.
(98) Jáky, M.; Szammer, J.; Simon-Trompler, E. Kinetics and mechanism of the oxidation of acetylacetone by permanganate ion. *Int. J. Chem. Kinet.* **2006**, *38* (7), 444−450.
(99) Ostrowska, K.; Kazmierska, A.; Rapała-Kozik, M.; Kalinowska-Tłuscik, J. Ratiometric fluorescent $Zn^{2+}$and In^{3+}receptors of fused pyrazine with an aminopropanol chain in acetonitrile. *New J. Chem.* **2014**, *38* (1), 213−226.
(100) Glatter, O. The interpretation of real-space information from small-angle scattering experiments. *J. Appl. Crystallogr.* **1979**, *12* (2), 166−175.
(101) Kojima, T.; Antonio, M. R.; Ozeki, T. Solvent-Driven Association and Dissociation of the Hydrogen-Bonded Protonated Decavanadates. *J. Am. Chem. Soc.* **2011**, *133* (19), 7248−7251.
(102) Bianconi, A.; Marcelli, A.; Dexpert, H.; Karnatak, R.; Kotani, A.; Jo, T.; Petiau, J. Specific intermediate-valence state of insulating 4f compounds detected by L_3 x-ray absorption. *Phys. Rev. B Condens. Matter.* **1987**, *35* (2), 806−812.
(103) Dexpert, H.; Karnatak, R. C.; Esteva, J. M.; Connerade, J. P.; Gasgnier, M.; Caro, P. E.; Albert, L. X-ray absorption studies of CeO_2, PrO_2, and TbO_2. II. Rare-earth valence state by L_{III} absorption edges. *Phys. Rev. B* **1987**, *36* (3), 1750−1753.
(104) Kaindl, G.; Wertheim, G. K.; Schmiester, G.; Sampathkumaran, E. V. Mixed valency versus covalency in rare-earth core-electron spectroscopy. *Phys. Rev. Lett.* **1987**, *58* (6), 606−609.
(105) Booth, C. H.; Walter, M. D.; Daniel, M.; Lukens, W. W.; Andersen, R. A. Self-contained Kondo effect in single molecules. *Phys. Rev. Lett.* **2005**, *95* (26), 267202.
(106) Joseph, B.; Torchio, R.; Benndorf, C.; Irifune, T.; Shinmei, T.; Pottgen, R.; Zerr, A. Experimental evidence of an electronic transition in CeP under pressure using Ce L_3 XAS. *Phys. Chem. Chem. Phys.* **2017**, *19* (27), 17526−17530.
(107) Lai, Y.; Bone, S. E.; Minasian, S.; Ferrier, M. G.; Lezama-Pacheco, J.; Mocko, V.; Ditter, A. S.; Kozimor, S. A.; Seidler, G. T.; Nelson, W. L.; Chiu, Y. C.; Huang, K.; Potter, W.; Graf, D.; Albrecht-Schmitt, T. E.; Baumbach, R. E. Ferromagnetic quantum critical point in $CePd_2P_2$with Pd →Ni substitution. *Phys. Rev. B* **2018**, *97* (22), 224406 DOI: 10.1103/PhysRevB.97.224406.

https://doi.org/10.1021/acs.inorgchem.3c02141
Inorg. Chem. XXXX, XXX, XXX−XXX